Microchemical Journal 124 (2016) 104–110

Contents lists available at ScienceDirect

Microchemical Journal

journal homepage: www.elsevier.com/locate/microc

Trace colorimetric detection of Pb^{2+} using plasmonic gold nanoparticles and silica–gold nanocomposites

Sheenam Thatai [a], Parul Khurana [a,b], Surendra Prasad [c,*], Sarvesh K. Soni [d], Dinesh Kumar [a,**]

[a] Department of Chemistry, Banasthali University, Banasthali 304022, Rajasthan, India
[b] Department of Chemistry, K.C. College, Churchgate, Mumbai 400020, India
[c] School of Biological and Chemical Sciences, Faculty of Science, Technology and Environment, The University of the South Pacific, Private Mail Bag, Suva, Fiji
[d] Centre for Advanced Materials and Industrial Chemistry, School of Applied Sciences, RMIT University, Melbourne, Australia

ARTICLE INFO

Article history:
Received 20 June 2015
Accepted 9 July 2015
Available online 21 July 2015

Keywords:
Pb^{2+} colorimetric detection
Plasmonic detection
Core–shell NCs
Plasmonic nanoparticles
Pb^{2+} ions

ABSTRACT

A novel, simple and highly sensitive plasmonic colorimetric method is developed for the detection of Pb^{2+} in aqueous samples. The method is based on the aggregation of gold nanoparticles (AuNPs) or SiO_{2core}–Au_{shell} nanocomposites (SiO_2@Au NCs) in the presence of Pb^{2+} ions. It was found that the colour of AuNPs or SiO_2@Au NCs changes in the presence of Pb^{2+} ions and the intensity of surface plasmon resonance (SPR) peak of AuNPs or SiO_2@Au NCs decreased. Thus, the synthesis of sensitive surface enhanced Raman scattering (SERS) materials; ~20 nm spherical AuNPs and ~360 nm SiO_2@Au NCs leads to the development of nanosensor for the detection of Pb^{2+} ions. Both AuNPs and SiO_2@Au NCs by virtue of their versatility show localized surface plasmon resonance (LSPR) peaks at 522 nm and 541 nm respectively. The synthesized AuNPs, SiO_2@Au NCs and analyte samples prepared were characterised using a scanning electron microscope, a transmission electron microscope and a UV–vis spectrophotometer. The SERS study was also used to compare sensitivities of both AuNPs and SiO_2@Au NCs towards Pb^{2+} ions using crystal violet (CV) as a target molecule. The analyte Pb^{2+} was detected as low as 500 nM using 20 nm AuNPs and 50 nM using 360 nm SiO_2@Au NCs. It was confirmed that SiO_2@Au NCs were found ten times more sensitive as compared to AuNPs for the detection of Pb^{2+} ions.

1. Introduction

Nanoparticles, notable for their small size, high surface area to volume ratios, and strong adsorption capacity, have been the subject of great interest in analytical chemistry [1]. The gold nanomaterials based optical probes have recently attracted considerable attention in the analysis of environmental and biological samples due to their simplicity, sensitivity and selectivity because of their unique size- and shape-dependent optical properties, high extinction coefficients and light scattering approaches [1–3]. Therefore, over the past decade, nanoparticles have widely been used for elemental detection, determination as well as speciation [1–3]. Nowadays most of the countries are facing shortage of safe potable water. In developing countries, the contamination of drinking water due to heavy metal ions like Pb^{2+}, Cd^{2+}, Zn^{2+} and As^{3+} from industrial effluents has been a challenging task before the analytical chemists [1–4]. The rapid progress in the field of nanotechnology and fabrication of advanced nanomaterials offers a range of applications including detection and remediation of a broad range of environmental contaminants [3,5,6]. Rapid, ultrasensitive and inexpensive analytical methods provide attractive tools for environmental monitoring [3,7–9]. The monitoring levels of potentially toxic metal ions like Hg^{2+}, Pb^{2+} and Cu^{2+} in aquatic ecosystems are extremely important as these ions have severe negative impacts on human health and the environment [1,10,11]. Among these metal ions, Pb^{2+} ions have received significant attention, largely because of the fact that it causes serious diseases like memory loss, anaemia, behaviour problems, low intelligence quotient and kidney dysfunction [13]. Due to its non-biodegradability even at low concentrations, Pb^{2+} ions can cause serious damage to the brain and central nervous system especially to children [14]. Therefore, the rapid, sensitive and trace level detection of Pb^{2+} ions is of great importance in public interest. While many effective fluorescent sensors have been successfully developed for various metal ions [15–19], there have been relatively few reports on Pb^{2+} ions sensing via selective fluorescent sensors [20–24].

Metallic nanoparticles (NPs), especially gold nanoparticles (AuNPs), have emerged and received much attention for colorimetric sensing of biomolecules and many heavy metal ions due to their high extinction coefficients, size and distance-dependent optical properties [1,2,25–29]. To successfully integrate these nanomaterials for the selective detection of different species, the surface of the AuNPs must first be functionalized with biomolecules or small receptors without altering the stability of the functional groups in solution [30–32]. Therefore, continued strategies have been develop metal ion sensors for specific

* Corresponding author. Tel.: +679 3232416; fax: +679 2321512.
** Corresponding author. Tel.: +91 9928108023; fax: +91 1438 228365.
E-mail addresses: prasad_su@usp.ac.fj (S. Prasad), dsbchoudhary2002@gmail.com (D. Kumar).

http://dx.doi.org/10.1016/j.microc.2015.07.006
0026-265X/

metals based on synthesis of nanomaterials. These are usually based on the localized surface plasmon resonance (LSPR) for the modified Au and even AgNPs [3,6–9,24,29–32]. Among various optical reporting methodologies listed in the literature for the detection of Pb^{2+} ions, sensing based on the plasmon absorption of Au and AgNPs is rather more promising [5,33,34]. Although in colorimetric assays AgNPs have been used less extensively in comparison to AuNPs, AgNPs also have shown its applicability for the heavy metal detection based on colour change between the dispersed and aggregated ones [3,35]. Triazocarboxyl AgNPs show a cooperative effect on the recognition of Co^{2+} over other metal ions tested [35] while mercapto pyridine glutathione-modified AuNPs were used as a colorimetric sensor for As^{3+} in groundwater [36]. Moreover, the metal NPs show excellent selectivity and sensitivity as colorimetric sensors when these are mostly of spherical morphology [3,11,12,19,35,36]. Simple, cost-effective and rapid colorimetric method for simultaneous detection of Hg^{2+}, Pb^{2+} and Cu^{2+} using papain enzyme-functionalized AuNPs has been developed with a detection limit of 200 nM [37]. One step synthesis of water soluble Au and AgNPs has also been reported at room temperature using a naturally occurring bifunctional molecule, i.e., gallic acid where ratiometric plots of the aggregated to the isolated forms are shown to have high sensitivity (30–300 μM) as well as selectivity for the naked eye detection of Pb^{2+} ions [38].

In our most recent reports, in addition to produce an excellent review on the analytical techniques involving NPs and core–shell nanocomposites as new generation water remediation materials [5], we have demonstrated not only the plasmonic detection of Fe^{3+} [8], F^- [39] and Cd^{2+} [40] but also the removal of F^- using nanomaterials from aqueous media [41–43]. We have also reported the development of promising surface enhanced Raman scattering (SERS) substrate: freckled SiO_2@Au nanocomposites [44]. Hence, in continuation of our interest in the application of nanomaterials [3,8,39–44], we report novel, efficient, rapid and visual detection method for Pb^{2+} ion based on the development of sensitive AuNPs and SiO_2@Au nanocomposites (SiO_2@Au NCs). Thus the present work describes the strategy for preparing citrate capped AuNPs and SiO_2@Au NCs based on a multistep process via a sol–gel reaction [45,46] in which the AuNPs were modified with silica and their applications for the detection of Pb^{2+} in aqueous samples.

2. Experimental

2.1. Materials

All the chemicals were of analytical reagent grade and used as received without any further purification. Tetraethoxysilane (TEOS, ≥99%), ethanol C_2H_5OH (≥99.5%), ammonium hydroxide (NH_4OH, ≥25% w/v in H_2O), tetrachloroauric acid trihydrate ($HAuCl_4 \cdot 3H_2O$, ≥99.99%), trisodium citrate dihydrate ($Na_3C_6H_5O_7 \cdot 2H_2O$, ≥99%), sodium borohydride ($NaBH_4$, ≥99.99%), 3-aminopropyltriethoxysilane (APTES, ≥99.9%), sodium hydroxide (NaOH pellets, ≥98.5%), silver nitrate ($AgNO_3$, ≥99%), lead chloride ($PbCl_2$, ≥99%), potassium carbonate (K_2CO_3, ≥99%) and crystal violet (CV) were all procured from Sigma-Aldrich (USA) and used in this study. Indium tin oxide (ITO) used in this study was obtained from Sigma Aldrich (USA) and used as such. Milli-Q purification system was used to get deionized water.

2.2. Instrumentation

The particle size analyses of AuNPs and SiO_2@Au NCs along with the morphological investigations have been made using a transmission electron microscope (TEM), a field emission scanning electron microscope (FESEM) and a scanning electron microscope (SEM) as per the requirements. The detection was also assessed using a UV–visible absorption spectrophotometer for surface plasmon resonance (SPR) and SERS. The absorption spectra were recorded on a UV-2401 spectrophotometer (Shimadzu) at room temperature. TEM measurements were performed on a Hitachi 2010 TEM (USA) operated at an accelerating voltage of 200 kV. SEM measurements were performed on JEOL XL30 SEM (USA) while FESEM images were obtained using a Hitachi S-4800 microscope (USA). Centrifugation was performed on a Sigma 3K15 centrifuge (USA). Raman spectra were recorded with a Renishaw 2000 equipped with Ar^+ ion laser (wavelength 532 nm) and a charge-coupled device (CCD) detector (Renishaw Co., U.K.). Samples for Raman spectroscopy studies were prepared on ITO slides obtained from Sigma Aldrich (USA).

2.3. Synthesis of AuNPs

The AuNPs were synthesized using citric acid colloidal reduction route [45,47]. Trisodium citrate (5 mL, 0.03 M) was added to boiling tetrachloroauric acid (10 mL, 5 mM) aqueous solution while stirring under reflux. The reaction mixture was kept boiling for 30 min when deep wine red colour was persisted, indicating the formation of the AuNPs. Thereafter heater was turned off, keeping the water condenser running till the NPs solution cooled down to room temperature. The AuNPs were isolated from the colloidal solution by centrifugation at 4000 rpm for 30 min and washed three times with 8 mL deionized water. The AuNPs thus obtained were dispersed in deionized Milli-Q water for further use.

2.4. Synthesis of SiO_2@Au nanocomposites

For the synthesis of SiO_2@Au nanocomposites it was essential to synthesize SiO_2 NPs. Silica NPs were synthesized by Stober's method where ethanol (15 mL), water (3 mL) and NH_4OH (0.75 mL) were mixed in a round bottom flask at room temperature and stirred for 30 min [48]. Then 1.2 mL of TEOS was added to above solution and stirred for 3 h. A white precipitate was obtained which was thoroughly washed three times with ethanol and dried. In order to get SiO_2@Au NCs, silica was initially functionalized using 12 mM APTES in C_2H_5OH:H_2O (3:1 v/v) and adding silica particles (0.04 mg in 4 mL alcohol) to APTES with APTES:silica ratio as 2.3:1 v/v. The resulting solution was vigorously stirred at 75 °C for 4 h. The solution was then centrifuged and the precipitate obtained was washed with water. The functionalized silica NPs were then re-dispersed in water.

The speckled SiO_2@Au NCs were synthesized in our three step procedure reported elsewhere [49]. In the first step, the gold seeds with silica particles were prepared. 20 mL (6.25 mM) of gold solution, 4.5 mL (0.1 M) of NaOH solution and 1 mL functionalized silica NPs in water were stirred at 75 °C for 10 min. This solution was centrifuged, washed with water and re-dispersed in 40 mL water. In the second step, gold hydroxide solution was prepared. For this 28 mg K_2CO_3, 100 mL of Milli-Q water and 1.5 mL of 25 mM gold sol solution were taken in a 250 mL round bottom flask, stirred and aged in the dark for 12 h. Finally, the solutions prepared in the 1st and 2nd steps were mixed and stirred for 10 min with (1.6 mL, 5.3 mM) $NaBH_4$ which led to the formation of water soluble plasmonic SiO_2@Au NCs.

2.5. Detection of Pb^{2+} ions

The stock solution of 1 mM $PbCl_2$ was prepared in Milli-Q water. 500 μL of each AuNP and SiO_2@Au NCs was taken separately in the different test tubes. 10, 100, 1000 and 2000 μL of Pb^{2+} of four different concentrations 50 nM, 5×10^2 nM, 5×10^3 nM and 10×10^4 nM were added in both AuNPs and SiO_2@Au NCs separately. For SERS activity, 1.5×10^{-2} mM concentration of CV was used where 10:1 dye to NP ratio was maintained. Each solution was subsequently subjected to various studies.

In order to find out limit of detection of Pb^{2+}, different concentrations of Pb^{2+} solutions containing 10, 100, 1000 and 2000 μL volumes were added separately into 500 μL AuNPs as well as SiO_2@Au systems. After thorough shaking, the colour changes in the solutions were

observed and UV–vis absorption spectra were recorded. TEM and SEM were used to measure the size of AuNPs and SiO_2@Au NCs also in the presence of Pb^{2+} and especially to monitor the amount of aggregation.

3. Results and discussion

In the past few years the metal NPs, due to their peculiar physical and chemical properties, have witnessed great potential in developing nanomaterials based optical sensing systems for the detection of various analytes such as metal ions, DNA, and proteins in a wide variety of samples [1–9]. The LSPR, which strongly depends on the shape, size and aggregation of NPs, is of great interest in detecting various species [3,7–9, 39,40]. The plasmonic based detection of Pb^{2+} ions is vital to field environment monitoring because of their toxic effects on the human health. Therefore it is extremely important to develop sensitive and reliable analytical tool for the detection of Pb^{2+} ions in water.

3.1. TEM/FESEM studies of AuNPs and SiO_2@Au NCs

The size of AuNPs and SiO_2@Au NCs was observed using electron microscopy. Fig. 1(A & B) represents the TEM images of AuNPs and silica particles respectively. The AuNPs were of quasi-spherical shape and SiO_2 NPs were of spherical shape. The average size of AuNPs and SiO_2 particles observed were ~20 nm and ~360 nm respectively.

Fig. 2 represents FESEM image of speckled SiO_2@Au NCs. It was observed that the average AuNPs size and silica particles were ~20 nm and ~320 nm, respectively, which got increased to ~360 nm after the decoration of AuNPs on silica particles i.e., after the formation of speckled SiO_2@Au core–shell NCs. The FESEM image clearly shows that the core–shell NCs synthesized herein were speckled particles i.e., they retain the gold particle size used in the formation of core–shell NCs. However, they appear as separate particles with certain nanogaps (1–2 nm) between them and create a large number of adsorption sites for the detection of Pb^{2+} ions.

3.2. Surface plasmon studies of AuNPs and SiO_2@Au NCs

The UV–vis spectra for AuNPs and SiO_2@Au core–shell NCs in solution are shown as Fig. 3. The UV–vis spectrum of AuNPs is sharper (a) compared to AuNPs on the SiO_2 NCs (b). The peak due to AuNPs was observed at ~522 nm due to surface plasmon resonance (SPR) absorption of NPs [40]. This peak at 522 nm is responsible for the ruby red colour displayed by conventional gold colloids. The SPR peak due to core–shell NCs appeared at 541 nm [40]. Thus there was a shift to the longer wavelength i.e., red shift in the case of SiO_2@Au core–shell NCs accompanied by broadening of the peak. This red-shift confirmed an enlargement of the NPs due to an increase in SiO_2@Au NC diameter.

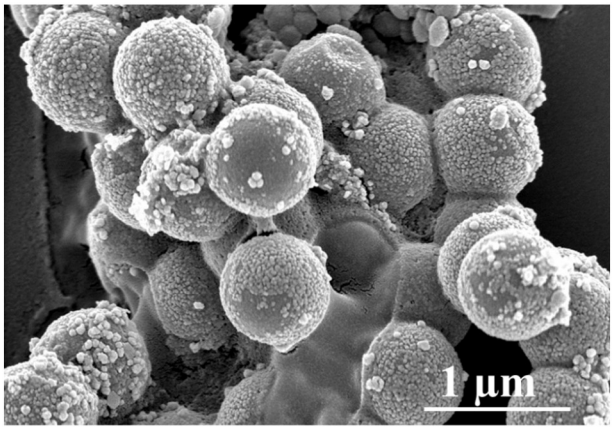

Fig. 2. Field emission scanning electron microscopy image of SiO_2@Au NCs.

The change in SPR position is also attributed to changes in the optical properties of the medium in which nanocomposite material was dispersed. The fact that the AuNPs are bound to the SiO_2 confirms that the red shifted peak evolved at 541 nm is due to aggregates of gold NPs [50–52].

3.3. Pb^{2+} ion detection and visual colour change

The surface plasmon peaks in UV–visible spectra of AuNPs, SiO_2@Au core–shell NCs and SiO_2@Au NCs along with increasing concentrations of Pb^{2+} are shown in Fig. 4. Fig. 4 clearly depicts that with increasing amount of Pb^{2+} in the solution of SiO_2@Au NCs, the intensity of the peaks decreased and at the highest concentration of Pb^{2+} the peak disappeared. It is also clearly shown that the peak width went on increasing with the increased addition of Pb^{2+} ions in the SiO_2@Au NC solution.

In Fig. 4, it was observed that changes in SPR spectra of SiO_2@Au NC solution occur at 50 nM concentration of Pb^{2+} ions which has a pronounced peak at 541 nm and its intensity dramatically decreased with increasing amount of Pb^{2+} ions but a sudden change was observed at 50 nM concentration. Thus, 50 nM was taken as the detection limit of Pb^{2+} using SiO_2@Au NCs. In addition, a red shift in SPR peak from 541–583 nm also took place which is clearly shown in Fig. 4. After the addition of 10×10^4 nM concentration of Pb^{2+} ions into NC solution, the characteristic peak completely disappeared; this might be due to the loss of the characteristic property of nano-regime after a strong aggregation of the SiO_2@Au NCs at this high concentration of Pb^{2+}.

In fact, the aggregation and corresponding colour change of nanoprobe solutions driven by target analytes have been employed for the visual detection of certain analytes, such as Cd^{2+} [40], F^- [39] and

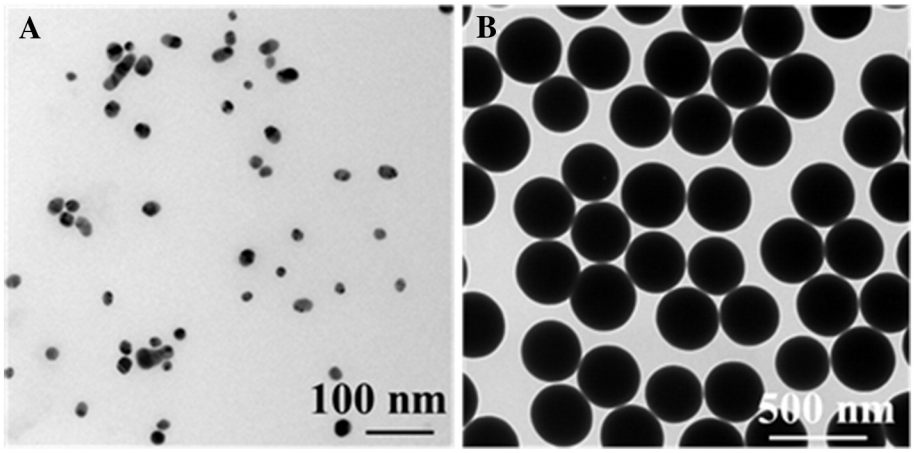

Fig. 1. Transmission electron microscopy images of (A) AuNPs and (B) SiO_2 particles.

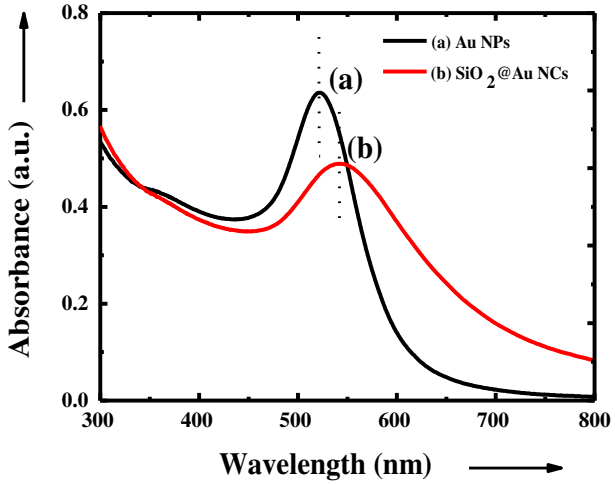

Fig. 3. UV–vis spectra of (a) gold nanoparticles and (b) silica gold nanocomposites i.e., SiO_2@Au NCs.

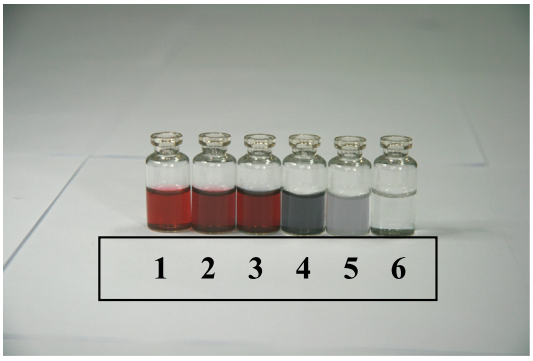

Fig. 5. Visual detection of SiO_2@Au NCs with different concentrations of Pb^{2+} (1) AuNPs, (2) SiO_2@Au NCs, (3) SiO_2@Au + 25 nM Pb^{2+}, (4) SiO_2@Au + 50 nM Pb^{2+}, (5) SiO_2@Au + 500 nM Pb^{2+} and (6) SiO_2@Au + 5×10^3 nM Pb^{2+} ions.

Fe^{3+} [8] and thus detection of Pb^{2+} ions in present study. Therefore, upon addition of Pb^{2+} ions the solution turned blue, induced by aggregation of SiO_2@Au NCs, which was detected by the naked eye and also confirmed by a red shift and broadened peak in the UV–vis spectra [53]. Thus Fig. 5 depicts a visual detection of 50 nm Pb^{2+} using SiO_2@Au NC solution which was also confirmed by the red shift in the SPR peak as shown in Fig. 4. Similarly, the change in the SPR peaks of AuNPs, with the addition of different amounts of Pb^{2+} was observed as shown in Fig. 6. The SPR peak of AuNPs appeared at 523 nm whose intensity started decreasing with the addition of Pb^{2+} and also showed red shift from 523 to 530 nm as shown in Fig. 6. A new peak at 693 nm also appeared and the red shift in band from 693–707 nm was clearly seen with the addition of 500 nM to 10×10^4 nM concentration of Pb^{2+} (Fig. 6).

3.4. SEM study on interaction of Pb^{2+} with NPs/NCs

The SEM observations indicated the formation of rod like shape in the sample of AuNPs upon addition of Pb^{2+} ions as has also been reported in the case of the detection of Fe^{3+} [8]. It also indicated that aggregating particles grow in a particular direction, and one dimensional growth of aggregating meta-stable spherical particles stabilized into nanorod shape which are the quintessential to show how optical properties are dependent on the dimensions (or shape) of NPs. Thus the dipole plasmon resonance of a solution of nanorods is typically split between transverse and longitudinal dipole resonances due to the different dimensions along the width and length of the particles and thus showing different peaks (Fig. 6). Therefore, the plasmon band of the resulting NPs red shifted with increasing concentration of Pb^{2+} ions.

To confirm the interaction of Pb^{2+} with SiO_2@Au, the SEM images of SiO_2@Au after the addition of 50 nM Pb^{2+} ions and also of AuNP solutions with 500 nM Pb^{2+} were taken as shown in Fig. 7 and Fig. 8(A & B) respectively. They also show different degrees of aggregation in the case of SiO_2@Au NCs and AuNPs in the presence of Pb^{2+}. Fig. 7 shows the SEM image of Pb^{2+} treated SiO_2@Au NCs and clearly shows very high degree of the aggregation in the sample i.e., SiO_2@Au NCs after the addition of 50 nM Pb^{2+}.

The formation of the aggregates in the case of AuNPs with 500 nM Pb^{2+} was also seen in the SEM images as shown in Fig. 8(A & B) and was in a linear fashion in the case of AuNPs which accounted for the appearance of the new peak in the range of 693–707 nm (cf. Fig. 6). Very dense aggregation with SiO_2@Au NCs was observed in the presence of 50 nM Pb^{2+} which was confirmed as the lower detection limit of Pb^{2+} by SiO_2@Au NCs in comparison to AuNPs.

The interaction of Pb^{2+} nanoprobes was also investigated using Raman spectroscopy as it is an excellent technique to investigate the interactions. The samples for the SERS study were prepared by mixing NPs

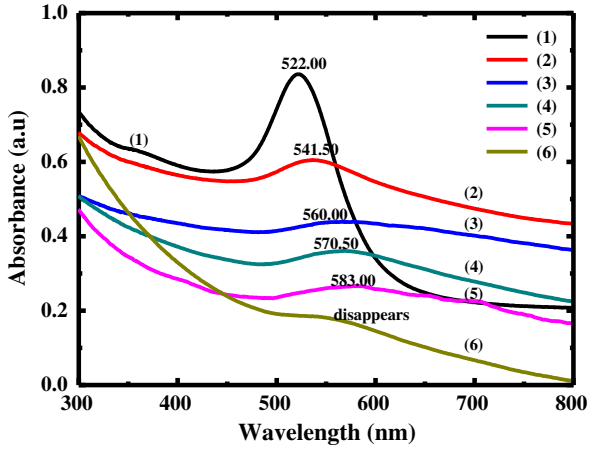

Fig. 4. Surface plasmon peaks in UV–visible absorption spectra of (1) AuNPs, (2) SiO_2@Au, (3) SiO_2@Au + 50 nM Pb^{2+}, (4) SiO_2@Au + 500 nM Pb^{2+}, (5) SiO_2@Au + 5×10^3 nM Pb^{2+} and (6) SiO_2@Au + 10×10^4 nM Pb^{2+}.

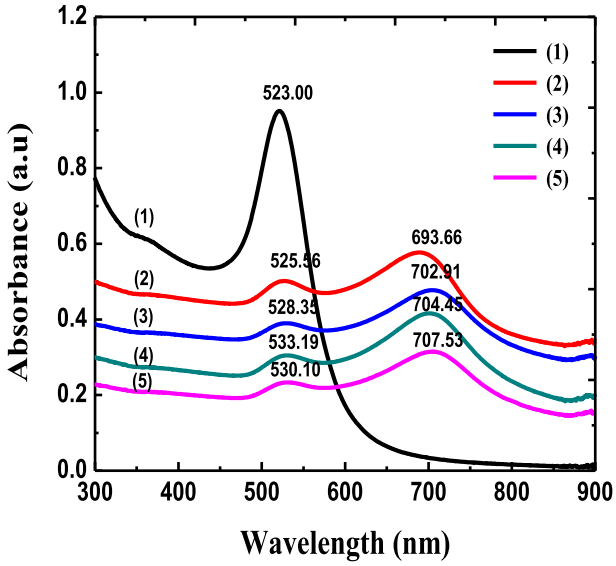

Fig. 6. SPR peaks of UV–visible absorption spectra of (1) AuNPs, (2) AuNPs + 50 nM Pb^{+2}, (3) AuNPs + 500 nM Pb^{2+}, (4) AuNPs + 5×10^3 nM Pb^{2+} and (5) AuNPs + 10×10^4 nM Pb^{2+}.

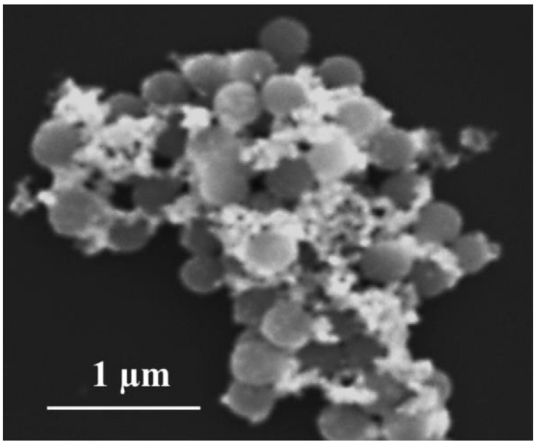

Fig. 7. Scanning electron microscopy image of SiO_2@Au core–shell NC solution after the addition of 50 nM Pb^{2+}.

or NC solutions with 10^{-4} M solution of CV and dropped on ITO substrate and dried for 12 h. Fig. 9(A) represents the effect on the SERS spectra by Pb^{2+} ions in SiO_2@Au NC solution obtained by using 10^{-4} M CV concentration, 0.05% laser power and at $\lambda = 532$ nm. On the other hand, Fig. 9(B) shows SERS spectra of AuNPs using CV (10^{-4} M) and 0.05% laser power.

The important observations from Fig. 9A & B have been obtained that both AuNPs and SiO_2@Au NCs coated ITO substrates did not give any detectable Raman signal. Similarly, CV molecules also do not show any Raman signal except one at ~500 cm^{-1} which is very clearly shown as spectrum 1 in Fig. 9A & B. However, when CV molecules are dispersed on AuNPs or SiO_2@Au NC surfaces, various vibrational modes (peaks) appeared with large intensity (cf. spectrum 2 in Fig. 9A & B). However, with the addition Pb^{2+} ions, the signal of CV molecules starts getting suppressed (spectra 3–6 in Fig. 9A & B). The reduction in the intensities in SERS spectra was consistent with the SPR observations i.e., SiO_2@Au was more sensitive compared to AuNPs (cf. Section 3.3). The SiO_2@Au NCs have also been reported as superior material as compared to AuNPs for the detection of Hg^{2+}, Pb^{2+} or Cu^{2+} [11]. Our most recent study on the detection of Cd^{2+} had also confirmed the similar conclusion [40].

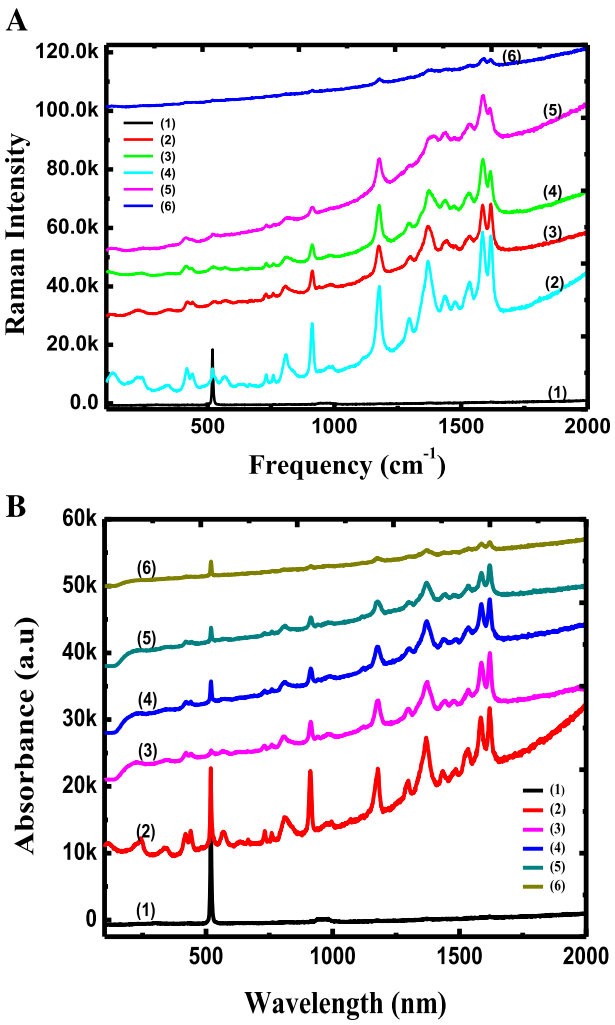

Fig 9. (A). SERS spectra of SiO_2@Au NCs solution using CV (10^{-4} M) as a model molecule and using 0.05% laser power (1) CV, (2) SiO_2@Au + CV, (3) CV + SiO_2@Au + 50 nM Pb^{2+}, (4) CV + SiO_2@Au + 500 nM Pb^{2+}, (5) CV + SiO_2@Au + 5×10^3 nM Pb^{2+}, (6) CV + SiO_2@Au + 10×10^4 nM Pb^{2+}. (B). SERS spectra of AuNPs using CV molecule (1) CV, (2) CV + AuNPs (3) CV + AuNPs + 50 nM Pb^{2+} (4) CV + AuNPs + 500 nM Pb^{2+}, (5) CV + AuNPs + 5×10^3 nM Pb^{2+} and (6) CV + AuNPs + 10×10^4 nM Pb^{2+}.

3.5. Comparison and selectivity

The proposed method was compared with other existing methods for the detection of Pb^{2+} ions. Table 1 represents the comparison of the limits of detection of various methods that have been developed involving nanomaterials as the nanoprobes [54–61]. The proposed method using SiO_2@Au NCs shows high selectivity and sensitivity for the naked eye detection up to 50 nM Pb^{2+} in water samples while 500 nM using AuNPs. Hence the synthesized SiO_2@Au core–shell NCs and AuNPs can play an important role as a SPR based sensor to detect a concentration of Pb^{2+} in aqueous samples in the range of 50–5000 nM and 500–10×10^4 nM respectively. Table 1 clearly shows that the proposed method using SiO_2@Au core–shell NCs is superior to many other methods due to its much lower limit of detection.

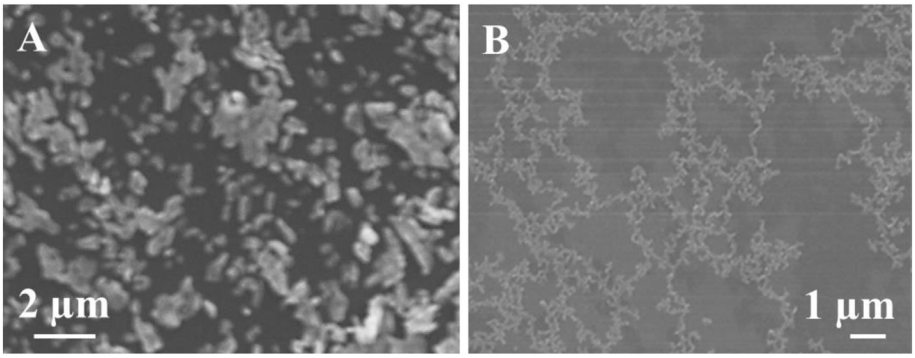

Fig. 8. (A & B). SEM images of aggregated AuNPs at 500 nM Pb^{2+}.

Table 1
Comparison of the limit of detection for Pb^{2+} involving different sensing materials.

Sensors for the detection of Pb^{2+}	Detection limit (μM)	Reference
2-Mercaptoisonicotinic acid functionalized AuNPs	0.1	[54]
Colorimetric detection of Pb^{2+} ions	0.5	[55]
L-Glutathione stabilized AuNPs	0.1	[56]
β-Cyclodextrin functionalized AuNPs	20	[57]
Alkyl phosphate functionalized AuNPs	1.7	[58]
Gold NPs	1.2	[59]
Sodium thiosulfate and hexadecyl trimethyl ammonium bromide modified AuNPs	0.1	[60]
Liquid metal marbles	10×10^3	[61]
Citrate capped plasmonic AuNPs	0.5	Present work
Plasmonic SiO_2@Au NCs	0.05	Present work

In terms of visual observation and real application of the proposed method to water samples, the selectivity is the most important characteristics of a colorimetric sensor. The colour of SiO_2@Au NC solution changes, from wine red to grey to light grey and finally colourless (Fig. 5) with increasing concentration of Pb^{2+} from 50, 500 to 5000 nM demonstrates its range and selectivity for the detection of Pb^{2+} in water samples.

4. Conclusion

The aggregate formation between Pb^{2+} ions with SiO_2@Au NCs or AuNPs was investigated by observing the change in SPR bands via UV–vis measurements and SEM studies. It has been confirmed that SiO_2@Au NCs were able to effectively detect 50 nM Pb^{2+} with the formation of large aggregates i.e., high degree of aggregation as compared to AuNPs with 500 nM. The largest shift in SPR bands with SiO_2@Au NCs at 50 nM Pb^{2+} while with AuNPs at 500 nM was confirmed by the SEM studies. The decrease in Raman intensities was observed and was consistent with the SPR observations i.e., SiO_2@Au NCs is more sensitive compared to AuNPs and showed the detection limit of 50 nM Pb^{2+}.

Acknowledgements

The authors acknowledge the successful collaboration with Prof. S. K. Kulkarni. DK would like to thank the University Grants Commission, New Delhi and Department of Science and Technology, Government of India, New Delhi, India while ST and PK thank Capital Normal University, Beijing, China for travel support. SP is grateful to the University of the South Pacific for support in various ways.

References

[1] C.-T. Liu, A.-N. Tang, Applications of nanoparticles in elemental speciation, Anal. Lett. 48 (2015) 1031–1043.
[2] L.-C. Ho, C.-W. Wang, P. Roy, H.-T. Chang, Sensitive and selective gold nanomaterials based optical probes, J. Chin. Chem. Soc. 61 (2014) 163–174.
[3] S. Thatai, P. Khurana, J. Boken, S. Prasad, D. Kumar, Nanoparticles and core–shell nanocomposite based new generation water remediation materials and analytical techniques: a review, Microchem. J. 116 (2014) 62–76.
[4] N. Parveen, Y. Rohan, Heavy metal contaminations in Sagar lake and drinking water sources of Sagar city, Int. J. Appl. Biol. Pharm. Technol. 3 (2012) 379–389.
[5] P. Biswas, C. Wu, Nanoparticles and the environment, J. Air Waste Manage. Assoc. 55 (2005) 708–746.
[6] A.K. Wanekaya, Applications of nanoscale carbon-based materials in heavy metal sensing and detection, Analyst 136 (2011) 4383–4391.
[7] K.M. Abu-Salah, S.A. Alrokyan, M.N. Khan, A.A. Ansari, Nanomaterials as analytical tools for genosensors, Sensors 10 (2010) 963–993.
[8] S. Thatai, P. Khurana, S. Prasad, D. Kumar, A new way in nanosensors: gold nanorods for sensing of Fe(III) ions in aqueous media, Microchem. J. 113 (2014) 77–82.
[9] S. Andreescu, O.A. Sadik, Trends and challenges in biochemical sensors for clinical and environmental monitoring, Pure Appl. Chem. 76 (2004) 861–878.
[10] K. Jomova, M. Morovi, Effect of heavy metal treatment on molecular changes in root tips of *Lupinus luteus* L. Czech J. Food Sci. 27 (2009) 386–389.
[11] Y. Guo, Z. Wang, W. Qub, H. Shaoa, X. Jiang, Colorimetric detection of mercury, lead and copper ions simultaneously using protein-functionalized gold nanoparticles, Biosens. Bioelectron. 26 (2011) 4064–4069.
[12] W. Xin, G. Xiangqun, Ultrasensitive Pb^{2+} detection based on fluorescence resonance energy transfer (FRET) between quantum dots and gold nanoparticles, Analyst 134 (2009) 1348–1354.
[13] C.-L. Li, C.-C. Huang, W.-H. Chen, C.-K. Chiang, H.-T. Chang, Peroxidase mimicking DNA–gold nanoparticles for fluorescence detection of the lead ions in blood, Analyst 137 (2012) 5222–5228.
[14] M.R. Knecht, M. Sethi, Bio-inspired colorimetric detection of Hg^{2+} and Pb^{2+} heavy metal ions using Au nanoparticles, Anal. Bioanal. Chem. 394 (2009) 33–46.
[15] A. Coskun, E.U. Akkaya, Ion sensing coupled to resonance energy transfer: a highly selective and sensitive ratiometric fluorescent chemosensor for Ag(I) by a modular approach, J. Am. Chem. Soc. 127 (2005) 10464–10465.
[16] T. Gunnlaugsson, T.C. Lee, R. Parkesh, Cd(II) sensing in water using novel aromatic iminodiacetate based fluorescent chemosensors, Org. Lett. 5 (2003) 4065–4068.
[17] Y. Leng, Y. Li, A. Gong, Z. Shen, L. Chen, A. Wu, Colorimetric response of dithizone product and hexadecyl trimethyl ammonium bromide modified gold nanoparticle dispersion to 10 types of heavy metal ions: understanding the involved molecules from experiment to simulation, Langmuir 29 (2013) 7591–7599.
[18] J. Liu, Y. Lu, Accelerated color change of gold nanoparticles assembled by DNAzymes for simple and fast colorimetric Pb^{2+} detection, J. Am. Chem. Soc. 126 (2004) 12298–12305.
[19] Y. Cho, S.S. Lee, J.H. Jung, Recyclable fluorimetric and colorimetric mercury-specific sensor using porphyrin-functionalized Au@SiO_2 core/shell nanoparticle, Analyst 135 (2010) 1551–1555.
[20] Y.W. Lin, C.C. Huang, H.T. Chang, Gold nanoparticle probes for the detection of mercury, lead and copper ions, Analyst 136 (2011) 863–871.
[21] Q. Zheng, C. Han, H. Li, Selective and efficient magnetic separation of Pb^{2+} *via* gold nanoparticle-based visual binding enrichment, Chem. Commun. 46 (2010) 7337–7339.
[22] Y. Wang, J. Irudayaraj, A SERS DNAzyme biosensor for lead ion detection, Chem. Commun. 47 (2011) 4394–4396.
[23] X. Miao, L. Ling, X. Shuai, Ultrasensitive detection of lead(II) with DNAzyme and gold nanoparticles probes by using a dynamic light scattering technique, Chem. Commun. 47 (2011) 4192–4194.
[24] Y.H. Chien, C.C. Huang, S.W. Wang, C.S. Yeh, Synthesis of nanoparticles: sunlight formation of gold nanodecahedra for ultra-sensitive lead-ion detection, Green Chem. 13 (2011) 1162–1166.
[25] H. Wang, L. Wang, K. Huang, S. Xu, H. Wang, L. Wang, Y. Liu, A highly sensitive and selective biosensing strategy for the detection of Pb^{2+} ions based on GR-5 DNAzyme functionalized AuNPs, New J. Chem. 37 (2013) 2557–2563.
[26] J. Lee, J.C. Park, H. Song, A nanoreactor framework of an Au@SiO_2 yolk/shell structure for catalytic reduction of p-nitrophenol, Adv. Mater. 20 (2008) 1523–1528.
[27] J. Nam, N. Won, H. Jin, H. Chung, S. Kim, pH-induced aggregation of gold nanoparticles for photothermal cancer therapy, J. Am. Chem. Soc. 131 (2009) 13639–13645.
[28] C.W. Liu, C.C. Huang, H.T. Chang, Highly selective DNA-based sensor for lead(II) and mercury(II) ions, Anal. Chem. 81 (2009) 2383–2387.
[29] H. Xu, B. Liu, Y. Chen, A colorimetric method for the determination of lead(II) ions using gold nanoparticles and a guanine-rich oligonucleotide, Microchim. Acta 177 (2012) 89–94.
[30] J. Liu, Y. Lu, Adenosine-dependent assembly of aptazyme-functionalized gold nanoparticles and its application as a colorimetric biosensor, Anal. Chem. 76 (2004) 1627–1632.
[31] H.-B. Wang, L. Wang, K.-J. Huang, S.-P. Xu, H.-Q. Wang, L.-L. Wanga, Y.-M. Liu, A highly sensitive and selective biosensing strategy for the detection of Pb^{2+} ions based on GR-5 DNAzyme functionalized AuNPs, New J. Chem. 37 (2013) 2557–2563.
[32] X. Mao, Z.P. Li, Z.Y. Tang, Adenosine-dependent assembly of aptazyme-functionalized gold nanoparticles and its application as a colorimetric biosensor, Front. Mater. Sci. 5 (2011) 322–328.
[33] Y. Kim, R.C. Johnson, J.T. Hupp, Gold nanoparticle-based sensing of "spectroscopically silent" heavy metal ions, Nano Lett. 1 (2001) 165–167.
[34] Y. Lu, J. Liu, Smart nanomaterials inspired by biology: dynamic assembly of error-free nanomaterials in response to multiple chemical and biological, Acc. Chem. Res. 40 (2007) 315–323.
[35] Y. Yao, D. Tian, H. Li, Cooperative binding of bifunctionalized and click-synthesized silver nanoparticles for colorimetric Co^{2+} sensing, ACS Appl. Mater. Interfaces 2 (2010) 684–690.
[36] R.J. Kalluri, T. Arbneshi, A.S. Khan, A. Neely, P. Candice, B. Varisli, M. Washington, S. McAfee, B. Robinson, S. Banerjee, A.K. Singh, D. Senapati, P.C. Ray, Use of gold nanoparticles in a simple colorimetric and ultrasensitive dynamic light scattering assay: selective detection of arsenic in groundwater, Angew. Chem. 48 (2009) 9668–9671.
[37] G. Yongming, W. Zhuo, Q. Weisi, S. Huawu, J. Xingyu, Colorimetric detection of mercury, lead and copper ions simultaneously using protein-functionalized gold nanoparticles, Biosens. Bioelectron. 26 (2011) 4064–4069.
[38] K. Yoosaf, B.I. Ipe, C.H. Suresh, K.G. Thomas, In situ synthesis of metal nanoparticles and selective naked-eye detection of lead ions from aqueous media, J. Phys. Chem. C 111 (2007) 12839–12847.
[39] J. Boken, S. Thatai, P. Khurana, S. Prasad, D. Kumar, Highly selective visual monitoring of hazardous fluoride ion in aqueous media using thiobarbituric-capped gold nanoparticles, Talanta 132 (2015) 278–284.
[40] S. Thatai, P. Khurana, S. Prasad, D. Kumar, Plasmonic detection of Cd^{2+} ions using surface-enhanced Raman scattering active core–shell nanocomposite, Talanta 134 (2015) 568–575.
[41] V. Tomar, S. Prasad, D. Kumar, Adsorptive removal of fluoride from aqueous media using *Citrus limonum* (lemon) leaf, Microchem. J. 112 (2013) 97–103.
[42] A. Dhillon, D. Kumar, Development of nanoporous adsorbent for the removal of health hazardous fluoride ions from aqueous systems, J. Mater. Chem. A 3 (2015) 4215–4228.

[43] V. Tomar, S. Prasad, D. Kumar, Adsorptive removal of fluoride from water samples using Zr–Mn composite material, Microchem. J. 111 (2013) 116–124.
[44] P. Khurana, S. Thatai, J. Boken, S. Prasad, D. Kumar, Development of promising surface enhanced Raman scattering substrate: freckled SiO2@Au nanocomposites, Microchem. J. 122 (2015) 45–49.
[45] C. Graf, D.L. Vossen, A. Imohof, A.V. Blaaderen, A general method to coat colloidal particles with silica, Langmuir 19 (2003) 6693–6700.
[46] Y. Pan, X. Du, F. Zhao, B. Xu, Magnetic nanoparticles for the manipulation of proteins and cells, Chem. Soc. Rev. 41 (2012) 2912–2942.
[47] V.G. Pol, A. Gedanken, J. Calderon-Moreno, Deposition of gold nanoparticles on silica spheres: a sonochemical approach, Chem. Mater. 15 (2003) 1111–1118.
[48] W. Stöber, A. Fink, E. Bohn, Controlled growth of monodisperse silica spheres in the micron size range, J. Colloid Interface Sci. 26 (1968) 62–69.
[49] P. Khurana, S. Thatai, P. Wang, P. Lihitkar, L. Zhang, Y. Fang, S.K. Kulkarni, Speckled SiO_2@Au core–shell particles as surface enhanced Raman scattering probes, Plasmonics 8 (2013) 185–191.
[50] L. Zhang, Y. Yao, J. Shan, H. Li, Lead(II) ion detection in surface water with pM sensitivity using aza-crown-ether-modified silver nanoparticles via dynamic light scattering, Nanotechnology 22 (2011) 275504–275511.
[51] Z. Wang, J.H. Lee, Y. Lu, Label-free colorimetric detection of lead ions with a nanomolar detection limit and tunable dynamic range by using gold nanoparticles and DNAzyme, Adv. Mater. 20 (2008) 3263–3267.
[52] H. Kuang, C. Xing, C. Hao, L. Liu, L. Wang, C. Xu, Rapid and highly sensitive detection of lead ions in drinking water based on a strip immunosensor, Sensors 13 (2013) 4214–4224.
[53] Y. Wen, F.Y. Li, X. Dong, J. Zhang, Q. Xiong, P. Chen, The electrical detection of lead ions using gold-nanoparticle and DNAzyme-functionalized graphene device, Adv. Healthcare Mater. 2 (2013) 271–274.
[54] E. Tan, P. Yin, X. Lang, H. Zhang, L. Guo, A novel surface-enhanced Raman scattering nanosensor for detecting heavy multiple metal ions based on 2-mercaptoisonicotinic acid functionalized gold nanoparticles, Spectrochim. Acta A 97 (2012) 1007–1012.
[55] P. Chen, R. Zhang, Q. Jiang, X. Xiong, S. Deng, Colorimetric detection of lead ion based on gold nanoparticles and lead-stabilized G-Quartet formation, J. Biomed. Sci. Eng. 8 (2015) 451–457.
[56] X. Mao, Z. Li, Z. Tang, One pot synthesis of monodispersed L-glutathione stabilized gold nanoparticles for the detection of Pb^{2+} ions, Front. Mater. Sci. 5 (2011) 322–328.
[57] B. Aswathy, G.S. Avadhani, S. Suji, G. Sony, Synthesis of β-cyclodextrin functionalized gold nanoparticles for the selective detection of Pb^{2+} ions from aqueous solution, Front. Mater. Sci. 6 (2012) 168–175.
[58] S.K. Kim, S. Kim, E.J. Hong, M.S. Han, Alkyl phosphate functionalized gold nanoparticles-based colorimetric probe for Pb^{2+} ions, Bull. Kor. Chem. Soc. 31 (2010) 3806–3808.
[59] J. Yang, C. Zhou, C. Liu, Y. Li, H. Liu, Y. Li, D. Zhu, A dual sensor of fluorescent and colorimetric for the rapid detection of lead, Analyst 137 (2012) 1446–1450.
[60] Y. Zhang, Y. Leng, L. Miao, J. Xin, A. Wu, The colorimetric detection of Pb^{2+} by using sodium thiosulfate and hexadecyl trimethyl ammonium bromide modified gold nanoparticles, Dalton Trans. 42 (2013) 5485–5490.
[61] V. Sivan, S.Y. Tang, A.P. O'Mullane, P. Petersen, N. Eshtiaghi, K. Kalantar-zadeh, A. Mitchell, Liquid metal marbles, Adv. Funct. Mater. 23 (2013) 144–152.